Structural characterization of a fluorescein hydrazone molecular switch with application towards logic gates

Article *in* New Journal of Chemistry · September 2018

DOI: 10.1039/C8NJ03817A

CITATIONS
0

READS
186

5 authors, including:

Richard Fernando D'vries
Universidad Santiago de Cali
56 PUBLICATIONS **374** CITATIONS

SEE PROFILE

Mario Alberto Macias
Los Andes University (Colombia)
75 PUBLICATIONS **154** CITATIONS

SEE PROFILE

NJC

PAPER

View Article Online
View Journal | View Issue

Cite this: *New J. Chem.*, 2018, **42**, 18050

Structural characterization of a fluorescein hydrazone molecular switch with application towards logic gates†

Juan D. Villada,[a] Richard F. D'Vries,[b] Mario Macías,[c] Fabio Zuluaga[a] and Manuel N. Chaur *[a]

A fluorescein acylhydrazone (**2**) and its metal complexes with Zn^{2+}, Ni^{2+} and Cu^{2+} ions were synthesized and characterized *via* NMR (^{1}H, ^{13}C and 2D experiments), UV-Vis, fluorescence, and FT-IR spectroscopy and single crystal X-ray diffraction. Compound **2** crystallizes in the $P\bar{1}$ triclinic space group with two fluorescein acylhydrazone (**2**) conformers and one water molecule per symmetric unit. The fluorescein acylhydrazone (**2**) and its metal derivates were analysed *via* cyclic voltammetry to determine the relationship between the shift in their redox potential upon the quenching of their fluorescence. Emission and UV-Vis absorption logic gates were fabricated based on the metal ion binding of **2** and its behaviour at different pH values. Compound **2** exhibited "on–off" behaviour in its fluorescence emission with the addition of triethylamine (TEA), and this effect was highly enhanced by the coaddition of Zn^{2+}. Conversely, its fluorescence is highly quenched by the addition of trifluoroacetic acid (TFA) or Ni^{2+} ions, which allows the fabrication of an AND gate using TEA and Zn^{2+} as inputs and an INHIBIT gate with the addition of TFA or Ni^{2+}, both using the fluorescence emission as outputs. The addition of Cu^{2+} results in a fluorescence emission at 525 nm, which is red-shifted with the addition of TEA. This behaviour allowed the construction of an XOR gate with the fluorescence emission at 525 nm as the output and the addition of Cu^{2+} and TEA as inputs. The absorption of **2** in the visible region was used to create AND gates with the addition of Cu^{2+} ions and TEA or Ni^{2+} and TEA as inputs. The INH, AND, XOR gates were manipulated by the controlled addition of different metal cations, TEA and TFA as inputs, and fluorescence emission and visible absorption as outputs, allowing the creation of three different combinatorial circuits, in which we highlight a new molecular switch "Half-Adder".

Received 31st July 2018,
Accepted 27th September 2018

DOI: 10.1039/c8nj03817a

rsc.li/njc

1. Introduction

The miniaturization of silicon semiconductors has resulted in the improvement of speed and computational capabilities of information devices.[1,2] In recent years, miniaturization processes have started to slow down due to quantum phenomena such as tunnelling currents and decrease in the breakdown voltages that impact the performance of semiconductors at the nanoscale. Considering this physical limitation, it is foreseeable that in a few years the miniaturization of information devices will be impossible, at least using semiconductor systems.[3] Accordingly, molecular switches are promising candidates for the replacement of silicon systems because their size is already in dimensions lower than the nanometer scale, their properties can be controlled from chemical modifications, and their manufacture is simple and easily scalable.[4]

Similarly to silicon systems, molecular switches receive information through external inputs (*e.g.*, pH changes, UV-Vis irradiation, and metal ions), then translate it into a binary language (0 = FALSE, OFF or 1 = TRUE, ON) and process it through different logic gates to generate a physical or chemical response (absorbance, fluorescence, potential, or current).[5] Several switches have been tested for the simple logic operations NOT, AND, and OR and even some complicated circuits such as Half-Adder and Half Subtractors.[6–12]

Most chemical logic systems are based on fluorophores and chromophores controlled by the attachment of different organic molecules.[13,14] These systems allow the design and

[a] *Facultad de Ciencias Naturales y Exactas, Departamento de Química, Universidad del Valle, A.A 25360, Cali, Colombia. E-mail: manuel.chaur@correounivalle.edu.co*
[b] *Facultad de Ciencias Básicas, Universidad Santiago de Cali, Calle 5 No 62-00, Cali, Colombia*
[c] *Departamento de Química, Universidad de los Andes, Carrera 1 No 18A-12, Bogotá, Colombia*

† Electronic supplementary information (ESI) available: Cyclic voltammetry, NMR spectra, crystallographic data and calibration curves. CCDC 1824290. For ESI and crystallographic data in CIF or other electronic format see DOI: 10.1039/c8nj03817a

synthesis of adaptable compounds capable of recognizing different inputs. Fluorescein derivatives are of great interest for the construction of these logic systems due to their photophysical properties (high extinction coefficient, excellent quantum yield and great photostability)[15–17] and the ability to tune them by structural modification. In fact, based on the spirolactam ring opening as the model for the design of fluorescein switches, multiple systems have been used for data processing and cation sensing.[18–21]

One of the most important challenges in the design of full molecular information devices is the communication among the systems. Thus, to address this issue, two different strategies have been used: (i) the combination of different molecular logic gates that can respond to the same chemical stimuli,[10,22] and (ii) the addition of different Boolean functions into the same molecule.[23] The latter can be achieved with molecules that can process different inputs simultaneously to produce different outputs, increasing the amount of data that can be processed by the molecular circuit.[24]

Molecular switches seem promising for the generation of computation at the nanoscale. However, the total replacement of semiconductors in electronic devices seems to be a long-term goal. For example, many of these molecular switches work in solution. This hurdle requires a big change in hardware development in order to be used for computational purposes.[25] Despite this, molecular switches that resemble the way biological systems handle information have become a new way to run computation in cells and different biological systems in which semiconductors cannot be used.

From this perspective, molecular switches are the ideal technology to process different chemical and biochemical signals with a highly specific response in biological systems. This ability has been used for sensing biological analytes,[26,27] in the diagnosis of different diseases,[28] and to generate new therapeutic systems.[29,30]

With this in mind, herein, we report the synthesis and electrochemical characterization of a fluorescein acylhydrazone (**2**) and the structural analysis of a new polymorph. This compound, which has been used as a fluorescent probe for cations and anions,[31] presents a hydrazone moiety capable of metal ion coordination,[32–35] which can be used as inputs in the design of logic gates. Furthermore, the presence of acidic protons on the structure allows even more control of the fluorescence emission and UV-Vis absorption for the integration of complex logical circuits, in which we highlight the design of the operator "Half-Adder".

2. Results and discussion

Molecular and supramolecular analysis

To obtain fluorescent switching behaviour, fluorescein hydrazine **1** was synthetized and reacted with 2-pyridinecarboxaldehyde to give the fluorescein-acylhydrazone **2** in 70% yield. The ^{13}C NMR spectra of **1** and **2** show a signal at 65 ppm, which corresponds to a quaternary aliphatic carbon, indicating the presence of the spiro group in the molecule (Fig. 1).

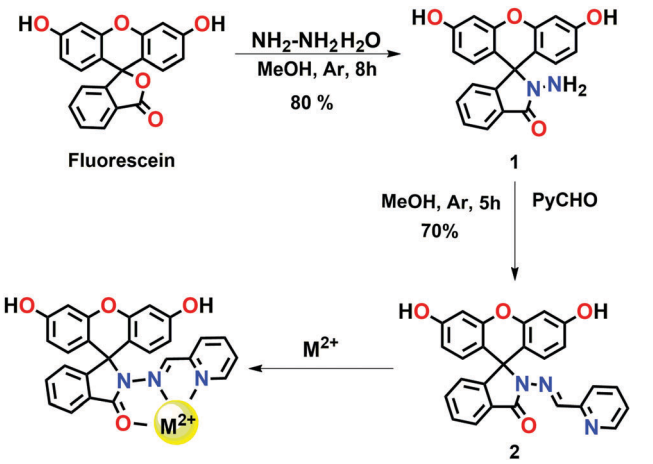

Fig. 1 Synthesis of fluorescein hydrazine (**2**) and its transition metal complexes.

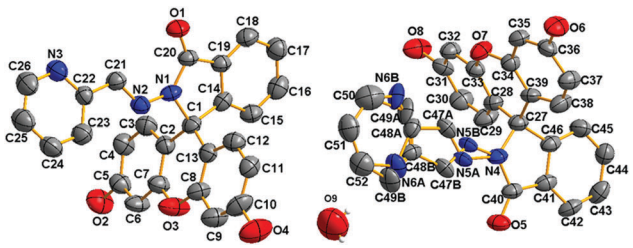

Fig. 2 Anisotropic displacement ellipsoid plots at 50% probability for the fluorescein-hydrazone compound.

The anisotropic displacement ellipsoid plots for compound **2** and the corresponding atomic numbering schemes are shown in Fig. 2. Details of the data collection, refinement and crystallographic data for this compound are summarized in Table S1 (ESI†).

Single crystals of fluorescein-acylhydrazone (compound **2**) were obtained by the slow evaporation of ethanol. Unlike the previously reported fluorescein molecule,[31] this compound crystallizes in the $P\bar{1}$ space group with two crystallographically independent molecules of fluorescein (conformers A and B) and one water molecule per unit cell (Fig. 3). Conformer A presents a greater torsion angle between the pyrrolidine ring and the pyridinyl hydrazone group with a torsion angle value of 22.1(8)° (C20–N1–N2–C22). Conformer B presents configurational disorder around the imine bond; therefore, a planar torsion angle is observed between the pyrrolidine ring and the pyridinyl hydrazone with values of 7.6(3) (C40–N4–N5B–C47B) and −176.2(1)° (C40–N4–N5A–C47A). This dynamic configurational disorder leads to a loss in planarity in the xanthene group going from 2.7(1)° for conformer A to 13.3(2)° for conformer B (Fig. 2). Also, as confirmed by ^{13}C NMR, the spiro group is present in the structure, where a comparative superposition near the spiro carbon shows a deviation in the atom positions in both conformers with an RMSD value of 0.9491 (Fig. 4).

Both conformers are joined by hydrogen bonds between the hydroxyl (conformer B) and carbonyl (conformer A) groups with

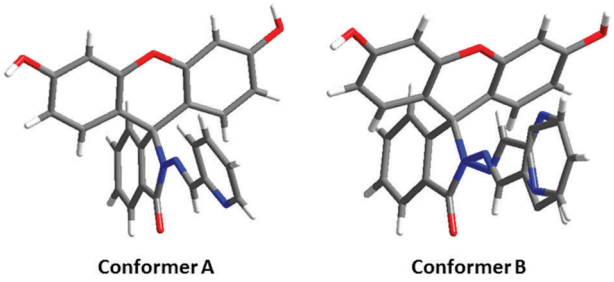

Fig. 3 Conformers A and B present in the unit cell.

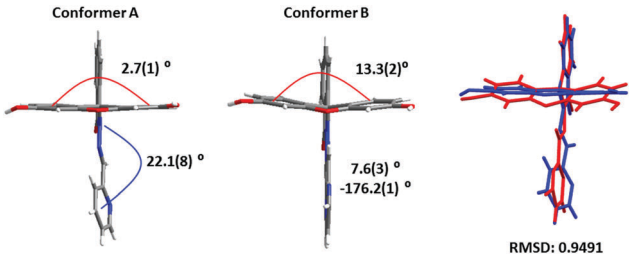

Fig. 4 Loss in planarity in xanthene in the molecules of conformers A and B present in the unit cell and superposition of both conformers (blue: conformer A; red: conformer B).

a distance O8–H8···O1 = 2.771(6) Å. Also, they are joined through a crystallization water molecule with distances O4–H4···O9 and O9–H9B···O5 = 2.699(1) and 2.860(2) Å and angles D–H···A of 157.8(6)° and 117.4(1)°, respectively. This arrangement gives rise to dimeric conformer subunits with an $R_3^2(22)$ graph-set representation of three donors and two acceptors ring set (Fig. 5).

Each dimeric subunit is joined along the [100] direction by O2H2···N3 and O6–H6···O5 hydrogen bonds with a distance of 2.925(8) and 2.828(7) Å, respectively. These interactions between the dimeric subunits give rise to supramolecular chains along the [100] direction (Fig. 6).

The 3D supramolecular structure can be explained in terms of weak C–H···A interactions and van der Waals interactions, which is possible to observe in the Hirshfeld analysis (HA)[36] (Fig. 7a). The HA is based in the analysis of interactions shorter than the sum of the van der Waals radii areas (d_{norm} Hirshfeld surface). This surface gives an idea of the donor and acceptor area in

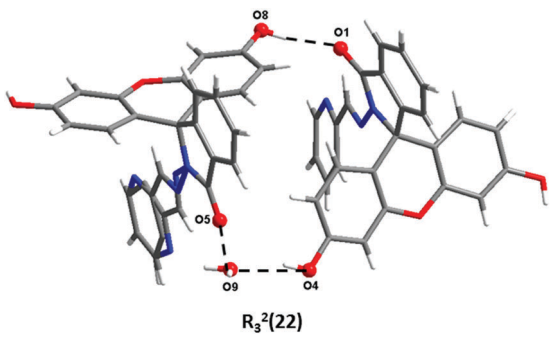

Fig. 5 Dimeric conformer subunits with an $R_3^2(22)$ graph-set representation of the three donors and two acceptors ring set.

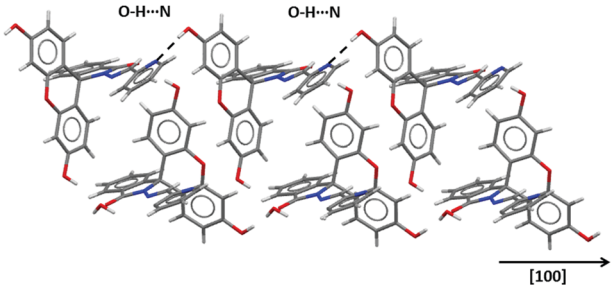

Fig. 6 Supramolecular chains formed along the [100] direction.

the molecule. Also, 2D-fingerprint plots are obtained from the Hirshfeld surface, which are used to quantify the interactions in a molecule.[37] In this case, the results of the HA and 2D-fingerprints plots show the significant presence of O···H/H···O and N···H/H···N interactions in each conformer and the dimeric subunits (Fig. 6). The mentioned interactions enable the formation of dimers and supramolecular chains. Weak C···H/H···C, H···H and C···C interactions are present in the crystal packing, which represent around of 70% of all the interactions.

A search in the CDS database showed us a report of one polymorph of the fluorescein acylhydrazone compound crystallising in the monoclinic space group *P*21/*c*, with two molecules of fluorescein acylhydrazone and one molecule of methanol in the asymmetric unit.[31,38] In this case, the superposition of both conformers present in the asymmetric unit shows more agreement between the atoms of the conformers with an RMSD value of 0.9771 (Fig. 8).

The crystalline behaviour of both polymorphs shows a significant difference in the crystal packing and molecular geometry. As is clearly noted, the obtained compound and that previously reported crystallize in different crystalline systems and space groups, indicating strong molecular differences that affect their crystal packing. As expected, in terms of supramolecular interactions, the QAVVAM whole molecule is governed by strong O···H/H···O and N···H/H···N interactions with values of 18.7% and 6.4%, respectively, and weak C···H/H···C, H···H and C···C interactions with a total value of around 71%, similarly with the values obtained for compound **2**.

Application as molecular logic gates

Fluorescein acylhydrazone **2** contains a binding pocket that can chelate different metal cations. The metal complexes formed with these cations produce different effects in its UV-Vis and fluorescence spectra. Furthermore, the acidic protons in the fluorescence moiety can be used to modulate the aforementioned responses, as has been studied by Huo *et al.*[31,38] This behaviour can be translated into a binary code and used in the generation of different logic gates. Additionally, by adding the chemical inputs in different orders, different gates can be linked together and used for the formation of complex logic circuits.

3-Input INHIBIT gate

Fluorescein acylhydrazone **2** works as an "OFF–ON" switch driven by the addition of a base (TEA), with the appearance of

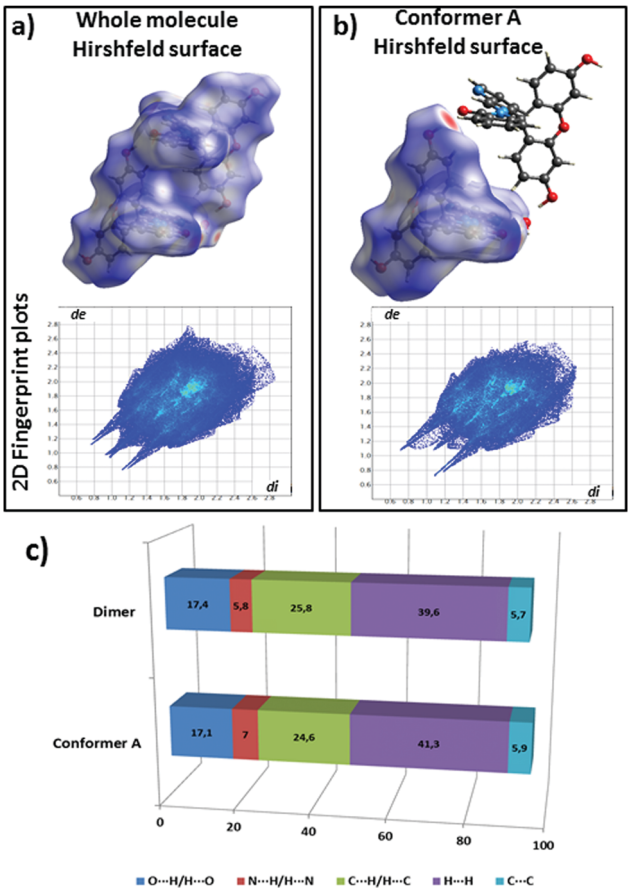

Fig. 7 (a) Whole molecule Hirshfeld surface and finger print plot, (b) conformer A HS and 2D FPP and (c) quantitative results of the interactions present in compound **2**.

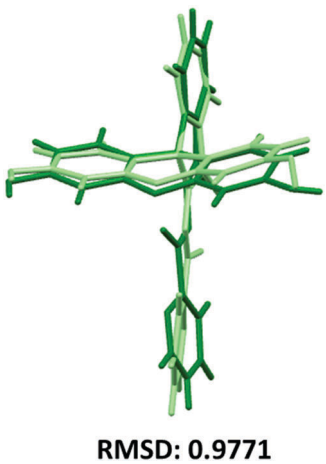

Fig. 8 Superposition of the conformers present in the compound QAVVAM.[31,38]

a fluorescence emission at around 525 nm. The emission can be enhanced by the addition of Zn^{2+} ions setting a threshold at QY = 0.10, and only the presence of TEA and Zn^{2+} will generate a "high" signal (Table 1) working as an AND gate. This gate requires both inputs to be present (1) for the output to be high (1),

Table 1 Truth table for the AND and INH logic gates fabricated with Zn^{2+}, TEA and TFA as inputs

Inputs			Output
TEA	TFA	Zn^{2+}	E_{525nm}
1	1	1	0 (0.01)
0	0	0	0 (0.01)
1	0	0	0 (0.07)
1	1	0	0 (0.01)
1	0	1	1 (0.15)
0	1	1	0 (0.01)

and any other combination will result in a low output (0), as seen in Table 1.

To increase the complexity of the logic circuit we can use the effect of acid media (TFA) to create an INHIBIT (INH) gate with the result of the AND gate. An INH gate can be simplified as a AND gate in which one of its inputs has been reversed (Fig. 9B). In our case, the fluorescence signal will be high when the base and the Zn^{2+} cation are both present, but the presence of TFA will block the base-related signal due to an acid–base reaction and will also make compound **2** release the metal *via* protonation of the pyridine ring.[32,39–41] This will inhibit the output signal, hence working as an INH function for the fluorescent output (Fig. 9B).

2 Inputs-INH and AND gate

The interaction between the Ni^{2+} cation and ligand **2** at high pH can be used to create a completely new combinatorial logical circuit using the absorbance as the output. This combinatorial circuit is based on a two input/two output system. The threshold for the fluorescent output is set at QY > 0.05 unlike in the last case to obtain a high signal (1) with the addition of TEA (Table 2). In this case the addition of Ni^{2+} will inhibit the fluorescence due to the charge transfer phenomena occurring between the protonated probe and the metal cation, resulting in an INH gate for the fluorescence emission (Fig. 10A). For this circuit, the absorbance band at 510 nm will be used as a second reading channel. The absorbance signal will be high (1 when $A > 0.5$) when both Ni^{2+} and TEA are present, creating an AND gate (Fig. 10B).

Half-Adder

Compound **2** behaves as a Half-Adder when the cation Cu^{2+} and base TEA are used as inputs and the fluorescence emission at 525 nm and the absorption band at 510 nm are used as output channels. A molecular Half-Adder is created by the combination of an XOR gate and an AND gate. The XOR or exclusive OR gate was created using the fluorescence emission at 525 nm. Notably, the emission is high (QY > 0.05) when one of the inputs (Cu^{2+} and TEA) is present, but low when both are present (Table 3). The AND gate was created using the UV-Vis absorption as the output. All possibilities for the inputs are listed in Table 3 and the combinatorial circuit in Fig. 11.

Table 3 shows that the interaction of the fluorescein hydrazone **2** with the Cu^{2+} cation results in an increase in fluorescence (QY 0.26). This enhancement has been observed in similar systems bearing fluorescein and rhodamine moieties.

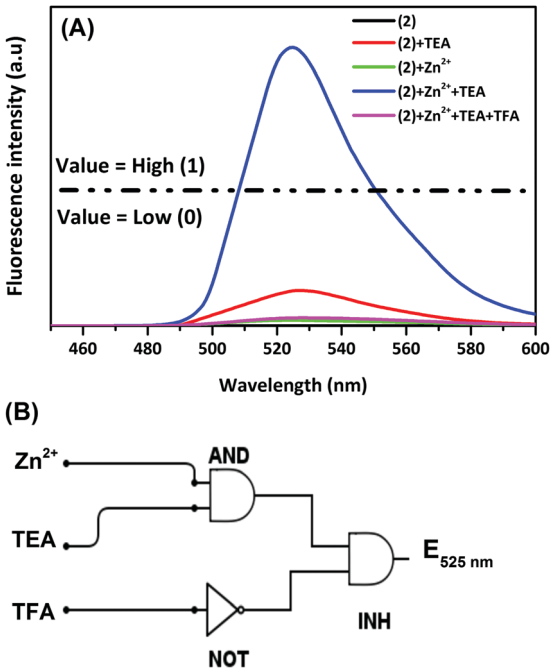

Fig. 9 (A) Three input AND/INHIBIT logic gates based on the acylhydrazone (**2**) when monitoring fluorescence at 525 nm and (B) schematic of the logical gate.

Table 2 Truth table for the AND and INH logic gates fabricated with Ni^{2+} and TEA as inputs

Input		Output	
TEA	Ni^{2+}	E_{525nm}	A_{510nm}
0	0	0 (0.01)	0 (0.00)
1	0	1 (0.07)	0 (0.06)
1	1	0 (0.01)	1 (1.09)
0	1	0 (0.01)	0 (0.00)

Those systems present spirocyclic rings, which are susceptible to present a ring opening fluorescent enhancement when grouped with the right metal cation. To prove this ring opening behaviour in our system, we ran different FT-IR experiments for the free ligand and the complexes formed with the different metal cations used in this work. The results show a decrease in the carbonyl stretching in the Cu^{2+} complex (see Fig. S13, ESI†). This behaviour is related with the ring opening of the organic ligand in the complex, which explains the fluorescence increase with the addition of Cu^{2+}.[42–45]

To be able to translate switching behaviour into a binary code, a threshold and a logical system must be set. In our systems, a positive logic was used. In this logic, a signal above the threshold will result in a positive signal ("1" or high).

On the other hand, different thresholds can be set to trigger different behaviours and to generate different circuits. In the case of the Half-Adder, a higher limit could be set to trigger a more specific signal for the fluorescence output, but it would be impossible to create the XOR gate, which is necessary for the development of the Half-Adder circuit.

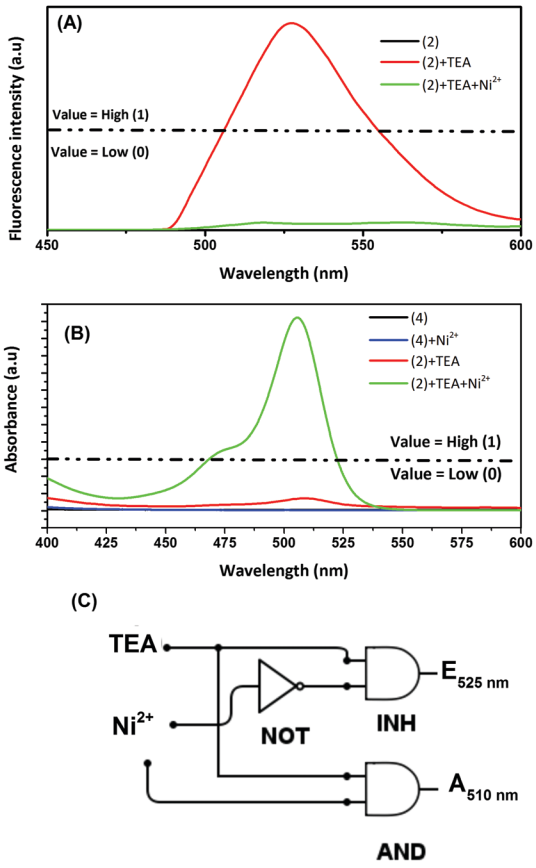

Fig. 10 (A) Two-input AND logic gate based on acylhydrazone (**2**) when monitoring fluorescence at 525 nm. (B) Two-input INH logic gate based on acylhydrazone (**2**) when monitoring absorbance at 510 nm. (C) Schematic of the logical gate.

Table 3 Truth table for the Half-Adder fabricated with Cu^{2+} and TEA as inputs

Input		Output	
TEA	Cu^{2+}	E_{525nm}	A_{510nm}
0	0	0 (0.01)	0 (0.00)
1	0	1 (0.07)	0 (0.08)
0	1	1 (0.26)	0 (0.08)
1	1	0 (0.01)	1 (1.64)

Half-Adders allow computational systems to mathematically perform the addition operation with different binary inputs to increase the signal or decrease a signal.[10] The binary numbers to be added are represented by the combination of Cu^{2+} and TEA as inputs. The result is read as a two bit number, *i.e.* 1 from the AND gate and 0 from the XOR gate, to give the answer 10, allowing the mathematical operation of both inputs, as in 1 + 1 = 10 (Table 3).[46,47]

Electrochemical behaviour

Cyclic voltammetry experiments were conducted in DMF with NBu_4PF_6 as the supporting electrolyte using a 3 mm-diameter glassy carbon disk as the working electrode, silver wire as the

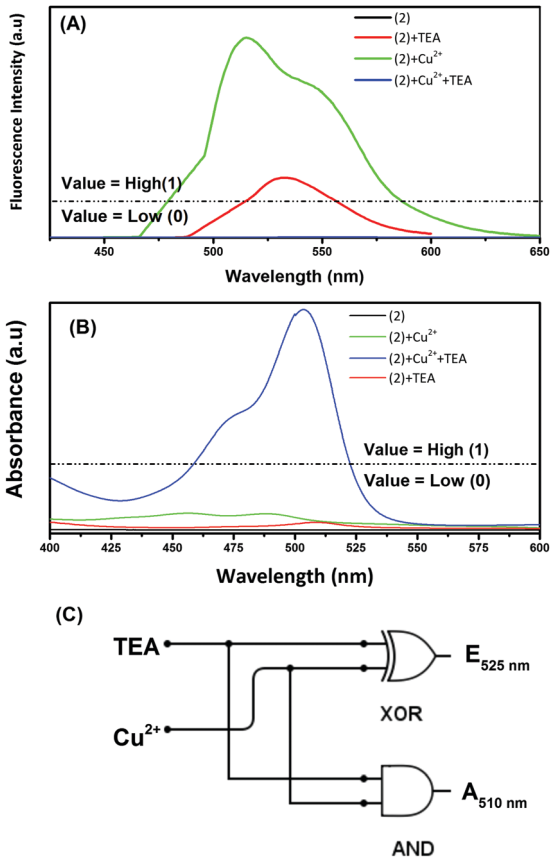

Fig. 11 (A) Two-input XOR logic gate based on acylhydrazone (**4**) when monitoring fluorescence at 525 nm. (B) Two-input AND logic gate based on acylhydrazone (**2**) when monitoring absorbance at 510 nm. (C) Schematic of the Half-Adder.

pseudo-reference electrode and platinum wire as the counter electrode. Ferrocene was added at the end of the experiments as an internal reference.

Table 4 shows the peak potentials of each cathodic and anodic event. Fluorescein and its derivatives **1** and **2** exhibit three irreversible reduction potentials (Fig. 12). These potentials are cathodically shifted for the derivatives due to the prevalence of the spiro isomer in these compounds. This moiety adds an sp^3 carbon to the structure, breaking the conjugation between the aromatic rings. Even if there is also a lactone form of fluorescein, which also presents a spirocyclic ring with an sp^3 carbon,

Table 4 Peak potentials in V for the cathodic and anodic events

Compound	$E_{p,Oxd(1)}$[a]	$E_{p,Red(1)}$[a]	$E_{p,Red(2)}$[a]	$E_{p,Red(3)}$[a]	$E_{p,Red(4)}$[a]	ΔE[b]
Fluorescein	—	—	−1.82	−2.69	−2.96	—
(**1**)	0.83	—	−2.80	−3.09	−3.51	−3.63
(**2**)	0.84	—	−2.24	−2.58	−3.3	−3.08
(**2**)-Zn	0.67	−1.35	−2.22	−2.57	—	−2.02
(**2**)-Ni	0.85	−1.47	−1.89	−2.50	−3.34	−2.32
(**2**)-Cu	0.91	−0.47	−1.81	−2.24	−2.48	−1.38

[a] Redox events are reported as peak potentials due to irreversibility of the events and are reported *vs.* ferrocene. [b] ΔE in volts calculated by the difference between the first oxidation potential minus the first reduction potential.

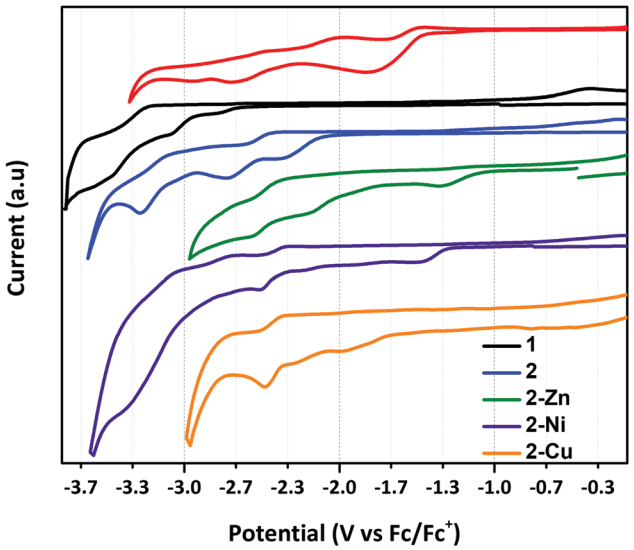

Fig. 12 Cyclic voltammograms of fluorescein, derivatives **1** and **2** and complexes (**2**) Zn, (**2**) Ni and (**2**) Cu. Solvent: DMF; electrolyte: $(n\text{-}Bu_4)NPF_6$; scan rate: 100 mV s^{-1}.

it is well-known that in solution, at neutral pH, the *p*-quinoid form is predominant over the lactone isomer.[48]

As is reported in the literature, the first reduction potential of compound **1** is attributable to the N atom with the lowest electron density in the (N–N) bond.[49] Even though the reduction of acylhydrazine is normally easier than normal hydrazones due to the presence of the electron withdrawing carbonyl; in the case of **1** the first reduction potential is at −2.80 V, and this highly negative reduction is related to the electron donor (–CH–) group bound to the nitrogen atom. The first reduction potential in compound **2** is anodically shifted compared with precursor **1**, suggesting that it may follow a different reduction mechanism. There are reports of hydrazones that undergo reduction on the imine (–C═N–) group, followed by stabilization *via* delocalization of the negative charge in the pyridine ring.[50,51] This stabilization may be the reason for the anodic shifting; however, future EPR studies should be carried out to confirm this hypothesis.

Complexation of **2** also alters the electrochemical behaviour. The first reduction peaks of complexes of **2** are anodically shifted compared with that of the free ligand. The metal cations have an electron withdrawing effect, which helps with the stabilization of the negative charge. The copper complex exhibits a reduction peak at −0.47 V, which is assigned to the reduction of Cu(II) to Cu(I) of the metal cation. After the reduction, the Cu(I) ions undergo chemical decomposition, which results in the deposition of metallic copper on the electrode.[52,53] This metallic copper oxidizes again at 0.15 V (see ESI†).

The reduction peaks of all the synthetized compounds were studied at different scan rates. The increase in the scan rates also increase the difference between the cathodic and anodic peak potentials, which is common in non-reversible events (ESI,† Fig. S7).

Compounds **1** and **2** present irreversible oxidation potentials at +0.83 V and +0.84 V, respectively, which are assigned to the

N–N bond.[54] These potentials remain almost constant with the complexation of Ni^{2+}, but shift cathodically in the Zn^{2+} complex and anodically in the Cu^{2+} complex. The difference in the oxidation potentials of the metal complexes reveals a different mechanism for the oxidation of these compounds. The oxidation potential is considered a rational principle in the prediction of fluorescein-like probes with high quantum yields. Nagano and co-workers proposed that fluorescein derivatives follow a fluorescence quenching mechanism based on a photoinduced electron transfer (PET) from the acyl benzene region to the xanthene-like fluorophore[55] due to the orthogonal position of these groups and the lack of ground state interaction between them.[56] For this reason, compounds with high oxidation potentials will have less PET and less fluorescence quenching. Actually, 1.23 V *vs.* Fc/Fc^+ (1.70 V *vs.* SCE) has been set as the threshold for high values of quantum yield.[56] Our compounds exhibit values lower than 0.91 V *vs.* Fc/Fc^+, which explain the low quantum yields of the synthetized compounds. From the analysis of the electrochemical band gaps, is it clear that the interaction with the metal cations results in a decrease in ΔE, which is presumably due to the electronic interactions between the ligand and the metal cation.

The full voltammograms can be found in the ESI† (Fig. S6). These experiments were performed in the cathodic direction, which resulted in the presence of an oxidation wave at around −0.5 V for all the compounds. This redox event is only present when the CV is taken in a cathodic direction and is an indication that the negatively charged species (radical or negatively charged) is very stable and that its re-oxidation follows a different mechanism.

The electrochemical studies show that there is a different response on the electrochemical gap, which depends on the nature of the metal cation. This gap is a hint of the behaviour of the HOMO–LUMO, which is an indication of how the metal cations affect the electronic orbitals and can explain the difference in the absorption and emission spectra used to develop the different logic gates.

3. Conclusions

A fluorescein acylhydrazone (**2**) and its M^{2+} (M = Zn, Ni and Cu) metal complexes were successfully synthesized and characterized. A new fluorescein acylhydrazone polymorph was obtained by slow solvent evaporation, which crystallizes in the $P\bar{1}$ triclinic space group. The asymmetric unit is formed by two conformer molecules of fluorescein acylhydrazone and one molecule of water. The Hirshfeld analysis reveals that the supramolecular structure of this compound is governed by O···H/H···O, N···H/H···N and weak H···H interactions.

The electrochemical properties show a cathodic shift of the first reduction potential of compounds **1** and **2** compared to the commercial fluorescein. This increases the ΔE, which may be related to the preference of these systems to stay in the spirocyclic forms. The anodic shift present in the complexes compared with the free ligand results in ΔE values closer to that found for commercial fluorescein, which explains the photophysical properties of these compounds. All our synthetized compounds exhibited low oxidation potentials, which are characteristic of systems in which the fluorescence is highly quenched by a photoinduced electron transfer mechanism, resulting in emissions of low quantum yields. The photophysical studies showed a wide range of behaviours of compound **2** and its metal complexes at neutral and basic pH. These responses were used in the design of several logic gates and combinatorial circuits, including a brand-new Half-Adder. The simplicity of its synthetic procedure and wide pool of interactions make our compound suitable for use in the design of information storage and processing devices.

4. Experimental

Materials and general methods

Reagents for the syntheses were purchased from Sigma Aldrich® and used without additional purification. FT-IR, NMR (1D and 2D experiments), UV-Vis, and fluorescence spectroscopy and elemental analysis were performed on a Shimadzu FTIR-8400 spectrophotometer, NMR 400 MHz Bruker Ultra Shield, Pharma Spec Shimadzu JASCO V-730 UV-VIS Spectrophotometer, JASCO FP-8500 Spectrofluorimeter, and Thermo FlashEA #1112 series instrument with a CHN analyser, respectively. Electrochemical experiments were performed on a three-electrode system using silver wire as the pseudo-reference electrode, platinum wire as the auxiliary electrode and glassy carbon as the working electrode. Peak potentials were reference *versus* ferrocene. All data was recorded on an Autolab PGSTAT302N potentiostat.

Single crystal structure determination

Single-crystal X-ray data for fluorescein-acylhydrazone was collected at room temperature on a Rigaku Oxford Diffraction SuperNova diffractometer using MoKα radiation (0.71073). Data reduction was carried out using CrysAlisPro.[57] The structure was solved using the SUPERFLIP software[58] and then refined by SHELXL-2014[59,60] included in WinGX[61] and Olex2.[62] Non-hydrogen atoms of the molecules were clearly resolved and full-matrix least-squares refinement with anisotropic thermal parameters was conducted. Aromatic and methyl hydrogen atoms were stereochemically positioned and refined with the riding model (with $U_{iso}(H) = 1.2U_{eq}$ and $1.5U_{eq}$). The anisotropic displacement ellipsoid plots were prepared with the Diamond[63] and Mercury[64] software packages. The TwinRotMat routine in the Platon software[65] was used to observe the presence of a twin and apply the twin law matrix (1 0 0, 0 1 0, 0 0 0) for the refinement of the structure.

Synthesis

Fluorescein hydrazine (1). A suspension of commercial fluorescein (519 mg, 1.56 mmol) in methanol was stirred for 10 minutes in reflux, then an excess of hydrazine monohydrate was slowly added to obtain a light orange solution, which was stirred under reflux. After 8 h, the excess hydrazine monohydrate was evaporated under reduced pressure. Compound **1** was

obtained as a light-yellow solid in 80% yield by precipitation using a mixture of EtOH/H_2O. ^{1}H-NMR (400 MHz, DMSO-d_6) δ: 9.82 (2H, s), 7.79–7.77 (1H, m), 7.51–7.46 (2H, m), 6.99 (1H, dd, J = 7.4, 5.1 Hz), 6.59 (2H, d, J = 1.8 Hz), 6.43 (4H, dt, J = 19.3, 5.2 Hz), 4.38 (2H, s). ^{13}C NMR (101 MHz, DMSO-d_6) δ = 165.9, 158.6, 152.8, 151.9, 133.1, 129.7, 128.8, 128.3, 123.8, 122.8, 112.4, 110.4, 102.8, 99.4, 65.1. M.p.: 256 °C. Elemental analysis: found C, 69.46; H, 4.27; N, 8.39 $C_{20}H_{14}N_2O_4$ calculated C, 69.36; H, 4.07; N, 8.09.

(2-Fluorescein-phenyl)-2-pyrinilhydrazone (2). 2-Pyridincarboxaldehyde (PyCHO) (100 μL, 1.05 mmol) was added to a stirring suspension of compound **1** (319 mg, 0.92 mmol) in ethanol to produce an orange suspension. The reaction mixture was stirred under reflux for 5 h. The orange solid was filtered from the crude of the reaction. Compound **2** was obtained as a white powder in 70% yield. Slow evaporation of an ethanol solution of **2** resulted in crystals suitable for X-ray diffraction. ^{1}H-NMR (400 MHz, DMSO-d_6) δ: 10.00 (2H, s), 8.54 (1H, s), 8.49 (1H, d, J = 4.5, 1.3 Hz), 7.97 (1H, dd, J = 7.8, 1.1 Hz), 7.80 (1H, td, J = 7.7, 1.7 Hz), 7.69–7.61 (3H, m), 7.34 (1H, ddd, J = 7.4, 4.8, 1.2 Hz), 7.13 (1H, d, J = 7.5 Hz), 6.70 (2H, d, J = 2.3 Hz), 6.55 (2H, d, J = 8.6 Hz), 6.48 (2H, dd, J = 8.6, 2.4 Hz). ^{13}C-NMR (101 MHz, DMSO-d_6) δ = 164.6, 159.2, 153.6, 152.3, 151.5, 149.9, 146.9, 137.4, 134.9, 129.6, 128.3, 128.2, 124.9, 124.1, 123.9, 119.6, 113.0, 109.9, 103.1, 65.3. M.p.: 335 °C. Elemental analysis: found: C, 71.70; H, 4.01; N, 9.68% $C_{26}H_{17}N_3O_4$ calculated C, 71.72; H, 3.94; N, 9.65%.

Transition metal complex preparation

Complexes of ligand **2** were obtained by adding a solution of the respective metal ion salt (8.4 mg of $Zn(BF_4)_2{\cdot}8H_2O$; $CuCl_2{\cdot}2H_2O$ and $NiCl_2{\cdot}6H_2O$ (0.022 mmol)) in 1 mL of ethanol to a stirring suspension of 10 mg of fluorescein-acylhydrazone (**2**) (0.022 mmol). The resulting solution was stirred for 24 h and a solid was obtained by the slow addition of diethyl ether.

2-Zn. A yellow powder was obtained by the slow evaporation of diethyl ether. ^{1}H-NMR (400 MHz, DMSO-d_6) δ: 9.97 (2H, s), 8.52 (1H, s), 8.47 (1H, d, J = 8.47 Hz), 7.94 (1H, d, J = 8.00 Hz), 7.78 (1H, m), 7.66–7.59 (3H, m), 7.32 (1H, m), 7.10 (1H, d, J = 7.10 Hz), 6.67 (2H, d, J = 8.6 Hz), 6.53 (2H, d J = 2.4 Hz), 6.45 (2H, dd, J = 8.6, 2.4 Hz). Elemental analysis: found C, 41.56; H, 2.88; N, 5.64. $[(C_{26}H_{17}N_3O_4)(Zn)(H_2O)_2](H_2O)_2\ (BF_4)_2$ calculated: C, 41.83; H, 3.38; N, 5.63.

2-Cu. A red-orange solid was obtained in 85% yield. ^{1}H-NMR (400 MHz, DMSO-d_6) δ/ppm: 9.97; 8.06; 7.72; 7.61; 7.24; 6.65; 6.41 (see Fig. S4, ESI†). Elemental analysis: found C, 51.55; H, 3.27; N, 6.79 for $[(C_{26}H_{17}N_3O_4)(Ni)(Cl_2)](H_2O)_2$ calculated: C, 51.54; H, 3.49; H, 1.01.

2-Ni. An orange powder was obtained by slow evaporation of diethyl ether in 90% yield. ^{1}H-NMR (400 MHz, DMSO-d_6) δ/ppm: 10.51; 10.01; 9.32; 8.50; 7.93; 7.64(m); 7.46(s); 7.31(m); 7.09; 6.84; 6.51; 6.47(d) (see Fig. S5, ESI†). Elemental analysis: found C, 50.29; H, 3.91; N, 6.44 $[(C_{26}H_{17}N_3O_4)(Ni)(Cl_2)](H_2O)_3$ calculated: C, 50.44; H, 3.74; N, 6.79.

Spectroscopic analysis.

Solutions of compound **2** and its metal complexes **2**-Zn, **2**-Ni, and **2**-Cu with an effective concentration of 50 μM in ethanol were used in the UV-Vis and emission studies at neutral pH. For the basic pH studies, a solution of 0.5 M of trimethylamine in ethanol was used as the solvent. Stock solutions of 1.56×10^2 M of $Zn(BF_4)_2$, $NiCl_2$ and $CuCl_2$ and 0.5 M of triethylamine (TEA) and trifluoroacetic acid (TFA) were used for the titration curves. All UV-Vis and emission spectra were measured in a quartz optical cell with a 1 cm optical path length at room temperature. The titration experiments with an increasing amount of TEA, TFA or metal cation solution of **2** or its metal complexes were maintained at 50 μM. Fluorescence experiments were carried out using an excitation wavelength of 490 nm.

Conflicts of interest

There are no conflicts to declare.

Acknowledgements

J. D. V. and M. N. C. are greatly thankful to the Vicerrectoria de Investigaciones and the Centro de Excelencia en Nuevos materiales (CENM) from the Universidad del Valle (Colombia) (71097) for the financial support of this work. Also COLCIENCIAS for the grant "Jovenes investigadores para la Paz" Convenio especial No. FP44842-407-2017. R. F. D. acknowledge to the Dirección General de Investigaciones (DGI) of the Universidad Santiago de Cali.

Notes and references

1 P. Gould, *Mater. Today*, 2005, **8**, 56–60.
2 G. E. Moore, *Electronics*, 1965, 114–117.
3 O. Bishop, *Electron. – Circuits Syst.*, 2011, 149–167.
4 R. F. Service, *Science*, 2002, **295**, 2398–2399.
5 A. P. de Silva and S. Uchiyama, *Nat. Nanotechnol.*, 2007, **2**, 399–410.
6 H. Chen, B. Zhou, R. Ye, J. Zhu and X. Bao, *Sens. Actuators, B*, 2017, **251**, 481–489.
7 H. Ding, G. Liu, S. Pu and C. Zheng, *Dyes Pigm.*, 2014, **103**, 82–88.
8 S. Pu, H. Ding, G. Liu, C. Zheng and H. Xu, *J. Phys. Chem. C*, 2014, **118**, 7010–7017.
9 Y.-S. Mi, D.-M. Liang, Y.-T. Chen, X.-B. Luo and J.-N. Xiang, *RSC Adv.*, 2014, **4**, 42337–42345.
10 G. J. Brown, A. P. de Silva and S. Pagliari, *Chem. Commun.*, 2002, 2461–2464.
11 A. P. De Silva, H. Q. N. Gunaratne and C. P. McCoy, *Nature*, 1993, **364**, 42–44.
12 S. Kou, N. L. Han, D. Van Noort, K. M. K. Swamy, H. K. So, H. S. Jung, K. M. Lee, S. W. Nam, J. Yoon and S. Park, *Angew. Chem., Int. Ed.*, 2008, **47**, 872–876.
13 A. P. de Silva, B. McCaughan, B. O. F. McKinney and M. Querol, *Dalton Trans.*, 2003, 1902–1913.
14 A. de Silva, *Coord. Chem. Rev.*, 2000, **205**, 41–57.

15 K. Chantalakana, N. Choengchan, P. Yingyuad and P. Thongyoo, *A highly selective 'turn-on' fluorescent sensor for Zn2+ based on fluorescein conjugates*, 2016, vol. 57.
16 J. M. Alvarez-pez, L. Ballesteros, E. Talavera and J. Yguerabide, *Methods*, 2001, 6320–6332.
17 F. A. Abebe, C. S. Eribal, G. Ramakrishna and E. Sinn, *Tetrahedron Lett.*, 2011, **52**, 5554–5558.
18 J. S. Wu, H. J. Kim, M. H. Lee, J. H. Yoon, J. H. Lee and J. S. Kim, *Tetrahedron Lett.*, 2007, **48**, 3159–3162.
19 L. Hou, J. Feng, Y. Wang, C. Dong, S. Shuang and Y. Wang, *Sens. Actuators, B*, 2017, **247**, 451–460.
20 H. Zheng, X.-Q. Zhan, Q.-N. Bian and X.-J. Zhang, *Chem. Commun.*, 2013, **49**, 429–447.
21 Q. A. Best, N. Sattenapally, D. J. Dyer, C. N. Scott and M. E. McCarroll, *J. Am. Chem. Soc.*, 2013, **135**, 13365–13370.
22 A. Prasanna de Silva and N. D. McClenaghan, *J. Am. Chem. Soc.*, 2000, **122**, 3965–3966.
23 A. P. De Silva, *Nat. Mater.*, 2005, **4**, 15–16.
24 D. Margulies, G. Melman and A. Shanzer, *J. Am. Chem. Soc.*, 2006, **128**, 4865–4871.
25 S. Erbas-Cakmak, S. Kolemen, A. C. Sedgwick, T. Gunnlaugsson, T. D. James, J. Yoon and E. U. Akkaya, *Chem. Soc. Rev.*, 2018, **47**, 2228–2248.
26 J. L. Klockow, K. S. Hettie and T. E. Glass, *ACS Chem. Neurosci.*, 2013, **4**, 1334–1338.
27 K. S. Hettie, J. L. Klockow and T. E. Glass, *J. Am. Chem. Soc.*, 2014, **136**, 4877–4880.
28 B. Rout, L. Unger, G. Armony, M. A. Iron and D. Margulies, *Angew. Chem., Int. Ed.*, 2012, **51**, 12477–12481.
29 Y. Benenson, B. Gil, U. Ben-Dor, R. Adar and E. Shapiro, *Nature*, 2004, **429**, 423–429.
30 B. A. Badeau, M. P. Comerford, C. K. Arakawa, J. A. Shadish and C. A. Deforest, *Nat. Chem.*, 2018, **10**, 251–258.
31 F. J. Huo, J. J. Zhang, Y. T. Yang, J. Bin Chao, C. X. Yin, Y. Bin Zhang and T. G. Chen, *Sens. Actuators, B*, 2012, **166–167**, 44–49.
32 M. N. Chaur, D. Collado and J.-M. Lehn, *Chem. – Eur. J.*, 2011, **17**, 248–258.
33 C. C. Carmona-Vargas, I. Y. Váquiro, L. M. Jaramillo-Gómez, J. M. Lehn and M. N. Chaur, *Inorg. Chim. Acta*, 2017, **468**, 131–139.
34 M. A. Fernandez, J. C. Barona, D. Polo-Cerón and M. N. Chaur, *Rev. Colomb. Quim.*, 2015, **43**, 5–11.
35 E. L. Romero, R. F. D'Vries, F. Zuluaga and M. N. Chaur, *J. Braz. Chem. Soc.*, 2015, **26**, 1265–1273.
36 J. J. McKinnon, M. A. Spackman and A. S. Mitchell, *Novel tools for visualizing and exploring intermolecular interactions in molecular crystals*, International Union of Crystallography, 2004, vol. 60.
37 M. A. Spackman and J. J. McKinnon, *CrystEngComm*, 2002, **4**, 378–392.
38 F.-J. Huo, C.-X. Yin, Y.-T. Yang, J. Su, J.-B. Chao and D.-S. Liu, *Anal. Chem.*, 2012, **84**, 2219–2223.
39 X. Su and I. Aprahamian, *Chem. Soc. Rev.*, 2014, **43**, 1963.
40 X. Su, T. Lessing and I. Aprahamian, *Beilstein J. Org. Chem.*, 2012, **8**, 872–876.
41 D. Ray, J. T. Foy, R. P. Hughes and I. Aprahamian, *Nat. Chem.*, 2012, **4**, 757–762.
42 X. Chen, T. Pradhan, F. Wang, J. S. Kim and J. Yoon, *Chem. Rev.*, 2012, **112**, 1910–1956.
43 J. W. Jeong, B. A. Rao and Y. A. Son, *Sens. Actuators, B*, 2015, **208**, 75–84.
44 B. Zhang, Q. Diao, P. Ma, X. Liu, D. Song and X. Wang, *Sens. Actuators, B*, 2016, **225**, 579–585.
45 J. W. Jeong, B. A. Rao, J. Y. Lee, J. Y. Hwang and Y. A. Son, *Sens. Actuators, B*, 2016, **227**, 227–241.
46 A. P. de Silva, N. D. McClenaghan and C. P. McCoy, *Mol. Switches*, 2001, **3**, 339–361.
47 D. H. Qu, Q. C. Wang and H. Tian, *Angew. Chem., Int. Ed.*, 2005, **44**, 5296–5299.
48 R. Sjöback, J. Nygren and M. Kubista, *Spectrochim. Acta, Part A*, 1995, **51**, L7–L21.
49 T. V. Tropol'skaya, E. N. Munin and Y. P. Kitaev, *Bull. Acad. Sci. USSR, Div. Chem. Sci.*, 1979, **28**, 919–925.
50 K. Polat, M. Uçar, M. L. Aksu and H. Ünver, *Can. J. Chem.*, 2004, **82**, 1150–1156.
51 J. M. W. Scott and W. H. Jura, *Can. J. Chem.*, 1967, **45**, 2377–2384.
52 S. Ilhan, H. Baykara, M. S. Seyitoglu, A. Levent, S. Özdemir, A. Dündar, A. Öztomsuk and M. H. Cornejo, *J. Mol. Struct.*, 2014, **1075**, 32–42.
53 M. Sönmez, M. Çelebi, A. Levent, İ. Berber and Z. Şentürk, *J. Coord. Chem.*, 2010, **63**, 1986–2001.
54 A. Adenier, M. M. Chehimi, I. Gallardo, J. Pinson and N. Vilà, *Langmuir*, 2004, **20**, 8243–8253.
55 T. Miura, Y. Urano, K. Tanaka, T. Nagano, K. Ohkubo and S. Fukuzumi, *J. Am. Chem. Soc.*, 2003, **125**, 8666–8671.
56 Y. Urano, M. Kamiya, K. Kanda, T. Ueno, K. Hirose and T. Nagano, *J. Am. Chem. Soc.*, 2005, **127**, 4888–4894.
57 Agilent, *CrysAlis PRO*, Agilent Technologies Ltd, Yarnton, Oxfordshire, England, 2014.
58 L. Palatinus and G. Chapuis, *J. Appl. Crystallogr.*, 2007, **40**, 786–790.
59 G. M. Sheldrick, *Acta Crystallogr., Sect. A: Found. Crystallogr.*, 2008, **64**, 112–122.
60 G. M. Sheldrick, *Acta Crystallogr.*, 2015, **71**, 3–8.
61 L. J. Farrugia, *J. Appl. Crystallogr.*, 2012, **45**, 849–854.
62 O. V. Dolomanov, L. J. Bourhis, R. J. Gildea, J. A. K. Howard and H. Puschmann, *J. Appl. Crystallogr.*, 2009, **42**, 339–341.
63 K. Brandenburg [or K. Brandenburg and H. Putz, or K. Brandenburg and M. Berndt], DIAMOND, Crystal Impact GbR, Bonn, Germany, 1999.
64 C. F. Macrae, I. J. Bruno, J. A. Chisholm, P. R. Edgington, P. McCabe, E. Pidcock, L. Rodriguez-Monge, R. Taylor, J. van de Streek and P. A. Wood, *J. Appl. Crystallogr.*, 2008, **41**, 466–470.
65 A. L. Spek, *Acta Crystallogr., Sect. D: Biol. Crystallogr.*, 2009, **65**, 148–155.

